Physics of the Earth and Planetary Interiors 204-205 (2012) 11–21

Contents lists available at SciVerse ScienceDirect

Physics of the Earth and Planetary Interiors

journal homepage: www.elsevier.com/locate/pepi

Does the Permo-Triassic geomagnetic dipole low exist?

Dunia Blanco [a,*], Vadim A. Kravchinsky [a], Jean-Pierre Valet [b], Arfan Ali [c], David K. Potter [a]

[a] Department of Physics, University of Alberta, Edmonton, Alberta, Canada T6G 2E1
[b] Institut de Physique du Globe de Paris, 1, Rue Jussieu, 75238 Paris Cedex 05, France
[c] Institute of Petroleum Engineering, Heriot-Watt University, Edinburgh EH14 4AS, United Kingdom

ARTICLE INFO

Article history:
Received 24 November 2011
Received in revised form 27 March 2012
Accepted 16 June 2012
Available online 23 June 2012
Edited by Mark Jellinek

Keywords:
Absolute paleointensity
Geomagnetic dipole
Permo-Triassic
Siberian flood basalts

ABSTRACT

Studies of absolute paleointensity have been conducted on specimens from Permo-Triassic sills from the eastern (areas of the kimberlite pipes Sytikanskaya, Yubileinaya and Aikhal) and northwestern (extrusions near Noril'sk city) parts of the Siberian platform. A total of 341 specimens have been subjected to a modified Thellier–Thellier technique which included partial thermoremanent magnetization checks and multidomain tail checks. The paleomagnetic directions derived from the present set of experiments ($D = 107.5°$, $I = 75.5°$, $k = 82.8$, $\alpha_{95} = 5.3°$, $N = 10$ sills, for the eastern localities and $D = 95.1°$, $I = 71.8°$, $k = 35.2$, $\alpha_{95} = 15.7°$, $N = 4$ outcrops, for the northwestern locality) agree with the directions from previous studies. The specimens from the northwestern sites (Noril'sk) did not provide any suitable result of absolute paleointensity. The mean virtual dipole moment obtained from only the eastern localities has a value close to $6.01 \pm 1.45 \times 10^{22}$ Am^2 which is over 50% higher than the results obtained by Heunemann et al. (2004) and Shcherbakova et al. (2005) on northwestern specimens. The discrepancy could possibly be explained by the presence of multidomain grains in northwestern specimens, where previous studies were undertaken, which would reduce the paleointensity estimates at high temperatures. However, the present results lead us to conclude that: (1) the geomagnetic field intensity at the Permo-Triassic boundary was very close to the observed present-day values and as a consequence a dipole low is not characteristic during this period of time; (2) the Mesozoic dipole low did not extend to the Permo-Triassic boundary, contrary to previous studies.

1. Introduction

Studies of absolute paleointensity provide important constraints to geodynamo models and a unique opportunity to document the evolution of the Earth's magnetic field over geological time. One of the best sources of information comes from long sequences of continental flood basalts (CFB). As these geological formations involve massive lava flows that are produced over relatively short time periods, they have recorded detailed information regarding the evolution of the field vector (Vandamme and Courtillot, 1992). The largest CFB is located on the north-western margin of the Siberian platform and is known as the Siberian trap basalt (STB, Fig. 1). Absolute dating indicates that the traps were intruded ~250 Myr ago (Courtillot and Renne, 2003; Almukhamedov et al., 2004; Reichow et al., 2005, 2009, and references therein) and generated huge volcanic activity over a very short period of time. A direct consequence is that it triggered the most massive extinction of flora and fauna known so far in Earth's history (Courtillot and Renne, 2003).

This is also a period of particular interest concerning the characteristics of the dipolar field between 200 Ma and 300 Ma. The few paleointensity studies that have been published for this specific period of time (Senanayake and McElhinny, 1983; Bol'shakov et al., 1989; Perrin et al., 1991; Solodovnikov, 1992, 1995; Thomas et al., 1995, 1997; Harcombe-Smee et al., 1996; Heunemann et al., 2004; Shcherbakova et al., 2005; Garcia et al., 2006) have shown paleointensity values lower than the present-day field. Further paleointensity data is required to determine whether Earth's dipole was weak at that period of time. Moreover, late Jurassic dipolar characteristics can be linked with the extension of the Mesozoic dipole low (MDL), a time interval characterized by a dipole which is thought not to have exceeded about 30% of the present field according to the records of absolute paleointensity that have been obtained by Prévot et al. (1990). Some studies (Bol'shakov and Solodovnikov, 1983; Tanaka et al., 1995; Perrin and Shcherbakov, 1997; Kosterov et al., 1998; Selkin and Tauxe, 2000; Zhu et al., 2001, 2003; Heller et al., 2002; Biggin and Thomas, 2003; Pan et al., 2004; Tarduno and Cottrell, 2005; Tauxe, 2006; Garcia et al., 2006; Shcherbakova et al., 2009; Brandt et al., 2009) are consistent with this observation, while other results (Goguitchaichvili et al., 2002, 2008; Ruiz et al., 2006) report higher paleointensity

* Corresponding author. Tel.: +1 780 492 5097; fax: +1 780 490 0714.
E-mail address: blancoac@ualberta.ca (D. Blanco).

0031-9201/$ - see front matter © 2012 Elsevier B.V. All rights reserved.
http://dx.doi.org/10.1016/j.pepi.2012.06.005

values and consider that the field at that time seems to have a similar variability to that of the present field.

Detailed records of paleointensity during the Permo-Triassic boundary would provide valuable information regarding the actual extension and characteristics of the dipole low. Two previous studies of absolute paleointensity (Heunemann et al., 2004; Shcherbakova et al., 2005) have been conducted in the STB at the Permo-Triassic boundary. Heunemann et al. (2004) used specimens from transitional sections and Shcherbakova et al. (2005) applied paleointensity studies to non-oriented specimens belonging to a stable period of the Earth's magnetic field based on previous work. Both studies involved sections from the northwestern part of the formation, and have indicated low virtual dipolar moments ($2.2 \pm 0.9 \times 10^{22}$ Am^2 and $2.9 \pm 2.3 \times 10^{22}$ Am^2, respectively). Our new study presents the first paleointensity data from oriented and non-transitional sections at the eastern part of the STB, which enables us to extend the paleointensity database for the Permo-Triassic boundary and verify if previous values are characteristic of the STB.

2. Geological settings

Absolute dating suggests a very narrow age interval (about one million years) when the Siberian traps were intruded at ~250 Ma, which corresponds to the Permo-Triassic boundary (PTB). The traps are found in the western part of the Siberian platform and under the West Siberian sedimentary basin and occupy an area of $\sim 3.7 \times 10^6$ km^2 with an approximate volcanic sequence thickness of 6.5 km and occupy a total volume of at least 3.0×10^6 km^3 (Kravchinsky et al., 2002; Reichow et al., 2009; Kuzmin et al., 2010).

Several models have been proposed to explain the emplacement mechanism of the traps. Some authors (Basu et al., 1998; Griffin et al., 1999; Courtillot et al., 1999) suggested that an upwelling mantle plume could create the rift system that led to the formation of the Siberian Traps. The Siberian trap magmatism is thought to be related to lithospheric break up linked to the mantle plume and not to plate boundary dynamics (Almukhamedov et al., 1996; Courtillot et al., 1999; Saunders et al., 2005; Kuzmin et al., 2010). Others (Elkins Tanton and Hager, 2000) proposed melt intrusions as the trigger for the eruption of the STB.

We analyzed specimens from the eastern and northwestern part of the STB (Fig. 1). In the eastern part ten extensive Permo-Triassic trap sills (5–20 m thick) have been studied in the areas of Sytikanskaya (66.11°N, 111.80°E), Yubileinaya (66.0°N, 111.7°E), and Aikhal (66.17°N, 111.33° E) kimberlite pipes. Paleomagnetic directions for three of the sills have been published by Kravchinsky et al. (2002). Sampling for both studies (Kravchinsky et al. (2002) and this study) was done in different parts of the kimberlite mine pit and outcrops nearby. The sampling locations were dependent upon mining progress and accessibility. It is common for smaller sills to branch out from the main sill intrusion and for the whole complex to occupy a few square kilometers. Although there are no absolute dates available for the Permo-Triassic traps, the sills cut through older, and are covered by younger, sediments. In some parts they also contain inclusions or lenses of the older sediments and fossils. The stratigraphic and age relations between sills are still unclear and it is commonly considered from the field observations that there were a few phases of eruption in the area. It is therefore thought that sampling of the different sills will average the secular geomagnetic variations and paleointensity results.

We also studied one extrusive trap multi flow outcrop in the area of the Noril'sk-Talnakh copper-nickel ore-mining district (69.21°N, 88.03°E), which is situated on the northwestern edge of the Siberian platform (Fig. 1). The district is located near the northwestern limit of the most extensive and relatively undisturbed exposures of STB. The basalt and dolerite specimens have been taken from six weakly mineralized and unmineralized more or less differentiated basalt sills south of Noril'sk. These intrusions have been correlated with stages of STB volcanism on the basis of cross-cutting relations, as well as geochemical and magnetic signatures (Dalrymple et al., 1995). Ergalakhsky type I, trachydolerite intrusions occur principally as shallow sills that were emplaced into friable sands and clays of the Upper Permian Tungusska Series (Dalrymple et al., 1995) in the central and southern parts of the Noril'sk area (location 2 on Fig. 1). On the basis of geologic mapping, their geochemical characteristics, and the fact that all other intrusion types cut them, they are considered to be coeval with the alkali trachybasalt flows of the Lower Ivakinsky subsuite.

3. Methodology

3.1. Magnetic Mineralogy

The magnetic mineralogy of the specimens has been investigated by Curie point thermomagnetic experiments and thermal dependent magnetic susceptibility (MS) measurements. The thermomagnetic experiments were performed in air using a Variable Field Translation Balance (VFTB), in a dwell field of 100 mT up to 705 °C. Thermal dependent MS was measured in air up to 700 °C using a Bartington furnace and susceptibility meter.

In order to determine the size of the magnetic carriers, hysteresis measurements at room temperature were applied on powdered specimens (mass 0.5 g) using the VFTB with a maximum applied field of 950 mT. Saturation magnetization (M_s), remanent saturation magnetization (M_{rs}), and coercive force (H_c) were determined after correcting for the paramagnetic contribution. The coercivity of remanence (H_{cr}) was calculated from backfield coercivity experiments, up to 959 mT. The thermal dependent MS measurements were performed in the Laboratory of Paleomagnetism and Petromagnetism of the University of Alberta (Edmonton, Canada) and all the VFTB measurements were done in the Petrophysics Laboratory at Heriot–Watt University (Edinburgh, United Kingdom).

3.2. Directions

Directional data for the STB has been previously studied by Kravchinsky et al. (2002) in the east of the province and by Pavlov et al. (2007) in the west of the province. In our study the paleomagnetic directions were obtained from thermal demagnetization in zero laboratory field during the paleointensity experiments described below. For both the directional analysis and paleointensity experiments we continuously monitored any mineralogical changes during the heating and cooling. Only a few specimens demonstrated such changes and therefore the directional analysis was reliable for most specimens. A total of 104 specimens from the northwestern locality and 237 specimens from the eastern localities were subject to this procedure up to a temperature of 580 °C.

The data were processed using Enkin (1996) and Cogné (2003) software. Demagnetization results were plotted on orthogonal vector endpoint diagrams (Zijderveld, 1967). Magnetization components were determined by principal component analysis (Kirschvink, 1980) and site-mean directions were calculated using Fisher (1953) statistics.

3.3. Absolute paleointensity

Measurements were carried out at the Laboratory of Paleomagnetism and Petromagnetism of the University of Alberta (Edmonton,

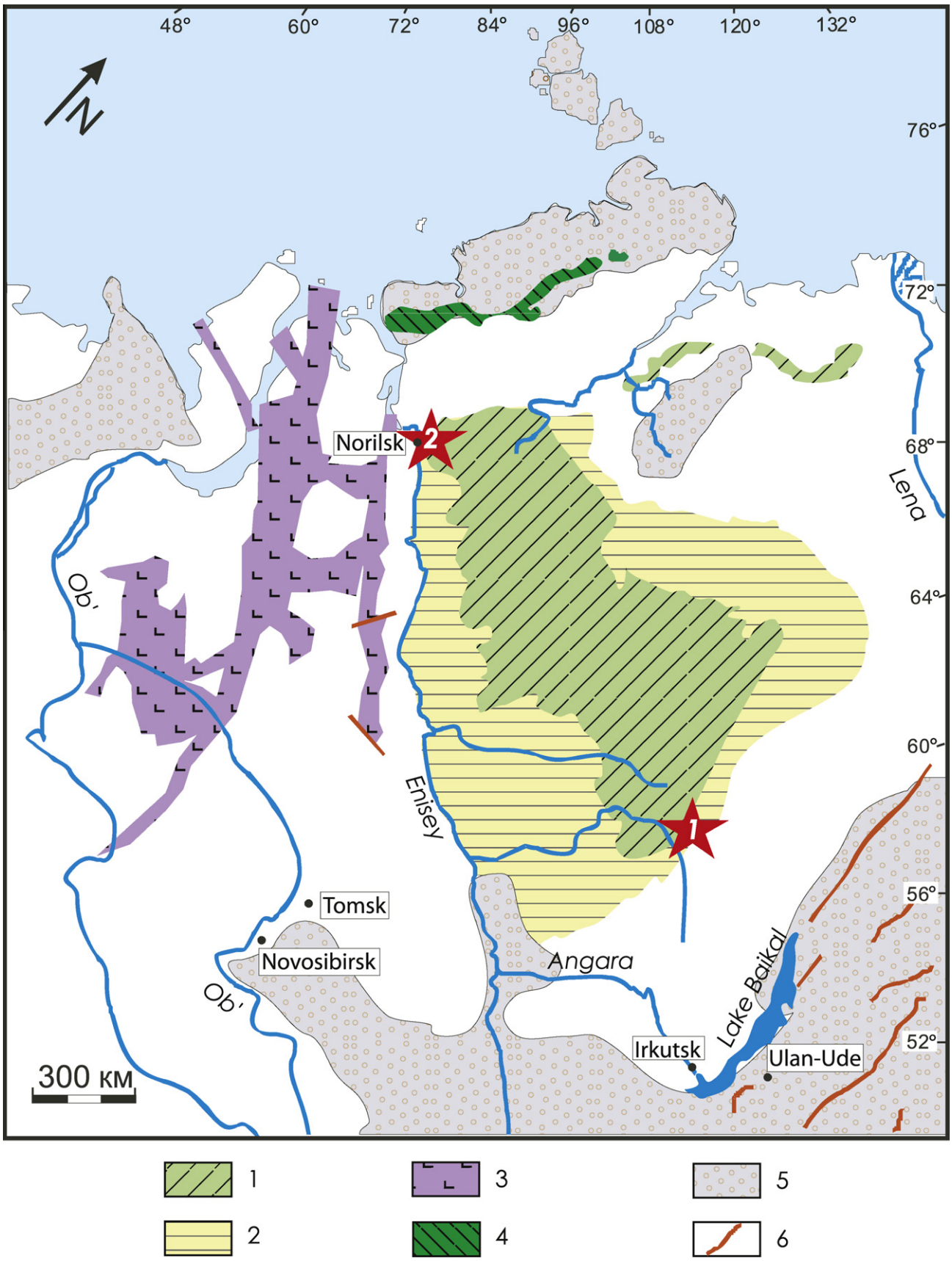

Fig. 1. Occurrences of the Late Permian – Early Triassic magmatism in the structures of the Siberian platform and West–Siberian plain (modified from Kuzmin et al., 2010). Our study areas are shown as red stars (1 – East Siberian intrusives, 2 – Noril'sk intrusion). 1 – extrusive volcanic rock exposure; 2 – intrusive volcanic rock exposure; 3 – West Siberian Rift basalts, tuffs, and tuffites; 4 – Taimyr Early Triassic traps; 5 – folded surrounding; 6 – major tectonic dislocations.

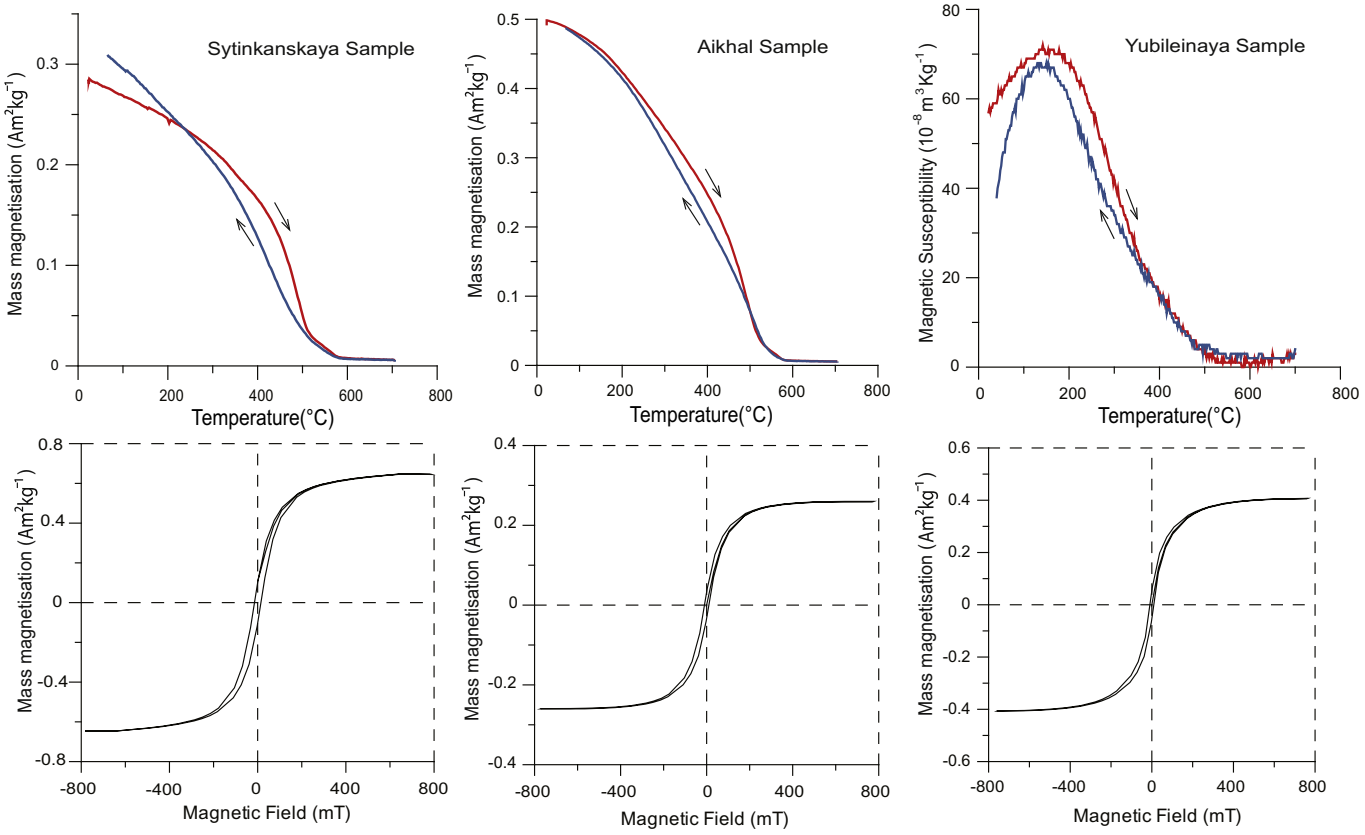

Fig. 2. Results of the rock magnetic experiments for specimens from Sytikanskaya, Aikhal and Yubileinaya, respectively. Top row: thermomagnetic curves (using the VFTB) and thermal dependent magnetic susceptibility (using the Bartington susceptibility meter). The red (blue) curves represent the heating (cooling) curves. Bottom row: magnetic hysteresis loops (using the VFTB). (For interpretation of the references to color in this figure legend, the reader is referred to the web version of this article.)

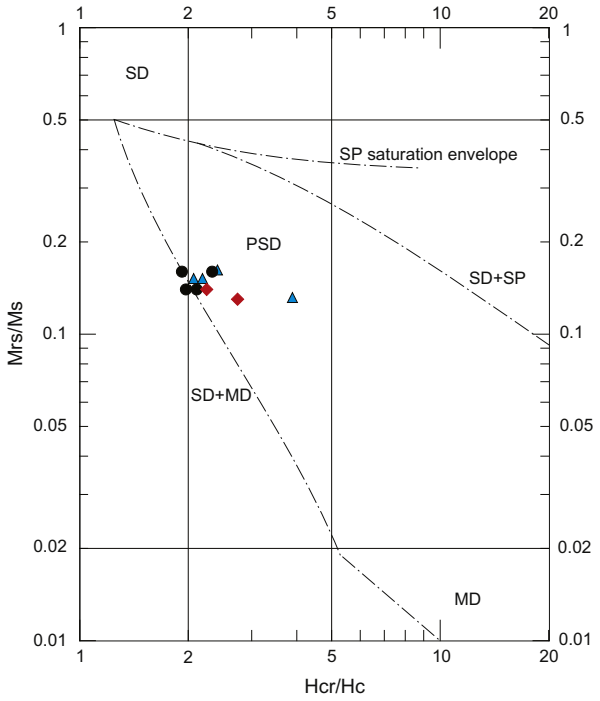

Fig. 3. Modified day diagram (based on Dunlop, 2002) of the hysteresis parameters at room temperature for Sytikanskaya (triangles), Aikhal (diamonds) and Yubileinaya (circles) localities. Magnetite SD + SP and SD + MD theoretical mixing lines of Dunlop (2002) are also shown (the fainter lines).

Canada) and at the Institut de Physique du Globe de Paris (France). Data from one set of specimens was acquired following the modified Coe version of the Thellier–Thellier technique (Coe, 1967). In this approach, the first heating step is then followed by cooling in zero magnetic field and the second heating step is followed by cooling in a known magnetic field, imparting a partial thermoremanent magnetization (pTRM) to the specimen (the so called ZI protocol). A slightly different protocol has been applied to another set of specimens. In this case pTRM was imparted before the demagnetization in zero field in order to test whether remagnetized components have been created in the presence of the field during the first heating (IZ protocol) (Aitken et al., 1988; Valet et al., 1998). Partial thermoremanent magnetization (pTRM) checks (Thellier and Thellier, 1959) were performed on all specimens and tail checks (McClelland and Briden, 1996; Riisager and Riisager, 2001) were applied only to specimens for which the intensity value was acquired following the standard Coe experimental protocol. In that case, after the double heating to T_i a third heating to T_i in zero laboratory field was performed. The tail check is the difference between the remanent magnetization of the two zero-field heatings.

The specimens were heated in a shielded ASC thermal demagnetizer (Edmonton) and a shielded Pyrox paleointensity furnace (Paris) and they were measured with 2G cryogenic magnetometers (both Edmonton and Paris). The field applied in the oven ranged between 20 and 80μT and we assumed that the acquired TRM is linearly proportional to a low applied magnetic field (such as the Earth's). The variation of TRM acquisition with applied field strength is beyond the scope of this study and we refer the reader to Selkin et al. (2007), Yu et al. (2007), and Shaar et al. (2010) for further discussion. However, our data do not present any evidence

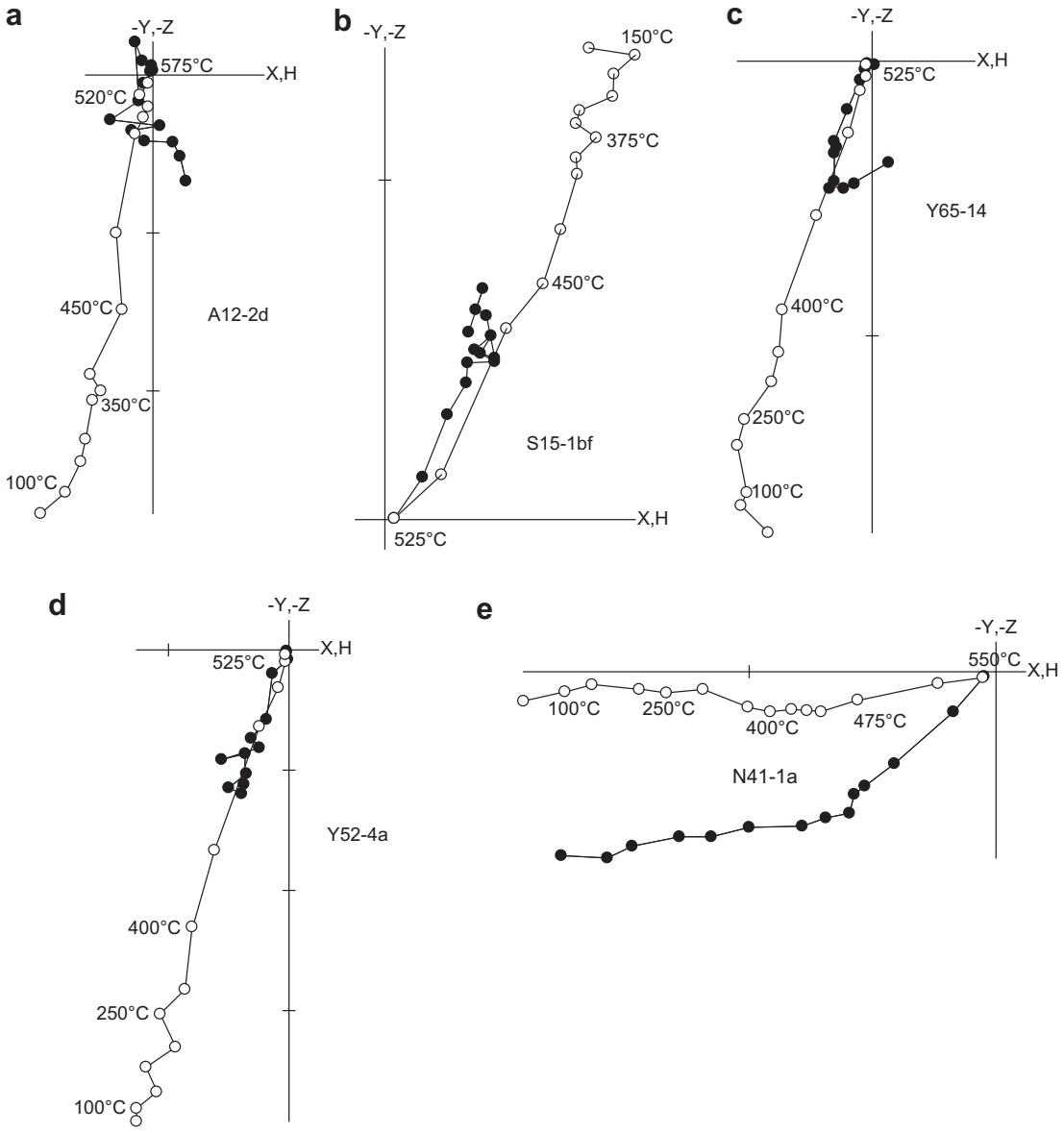

Fig. 4. Representative vector end-point diagrams of stepwise thermal demagnetization of natural remanent magnetization for the studied localities. Demagnetization steps are in °C, open and solid circles represent vector endpoints projected onto the vertical and horizontal planes, respectively. (a) Aikhal, (b) Sytikanskaya, (c, d) Yubileinaya, and (e) Noril'sk.

of a dependence of the average ancient field on the applied laboratory field. All specimens were heated and cooled in air. A total of 341 oriented cubic specimens with side length between 0.7 and 1 cm were subjected to paleointensity experiments.

The selection of appropriate specimens for the calculation of absolute paleointensity has been achieved using several successive steps, the more important ones are summarized below:

1. The quality of the demagnetization diagrams of the NRM was considered as a prerequisite to any interpretation. Only diagrams characterized by a linear decrease of the magnetic moment towards the origin have been considered. The specimens were always placed in the oven at exactly the same location with the same orientation relative to the applied magnetic field. This enabled us to monitor the presence or absence of remagnetization in the direction of the field within the oven when analyzing the directions.
2. The length of the linear segment (fraction of NRM, *f*) isolated from the Arai plots is critical to provide a suitable determination of absolute paleointensity. Recent results (Herrero–Bervera and Valet, 2009; Valet et al., 2010) have shown that specimens characterized by a sharp decrease of most of their NRM over a very narrow range of high temperatures are the most appropriate for successful determinations of paleointensity. Following the most recent suggestions on this matter (Valet et al., 2010) it is reasonable to consider that at least 60% of the magnetization should be incorporated in the segment defining the slope of the NRM–TRM plot.
3. Positive pTRM and tail checks indicate the absence of alteration and mineralogical changes produced during successive heatings. However, experimental uncertainties may affect the repeatability of the measurements so that quantitative factors are appropriate to determine a limit beyond which two successive measurements of pTRMs should be considered as being

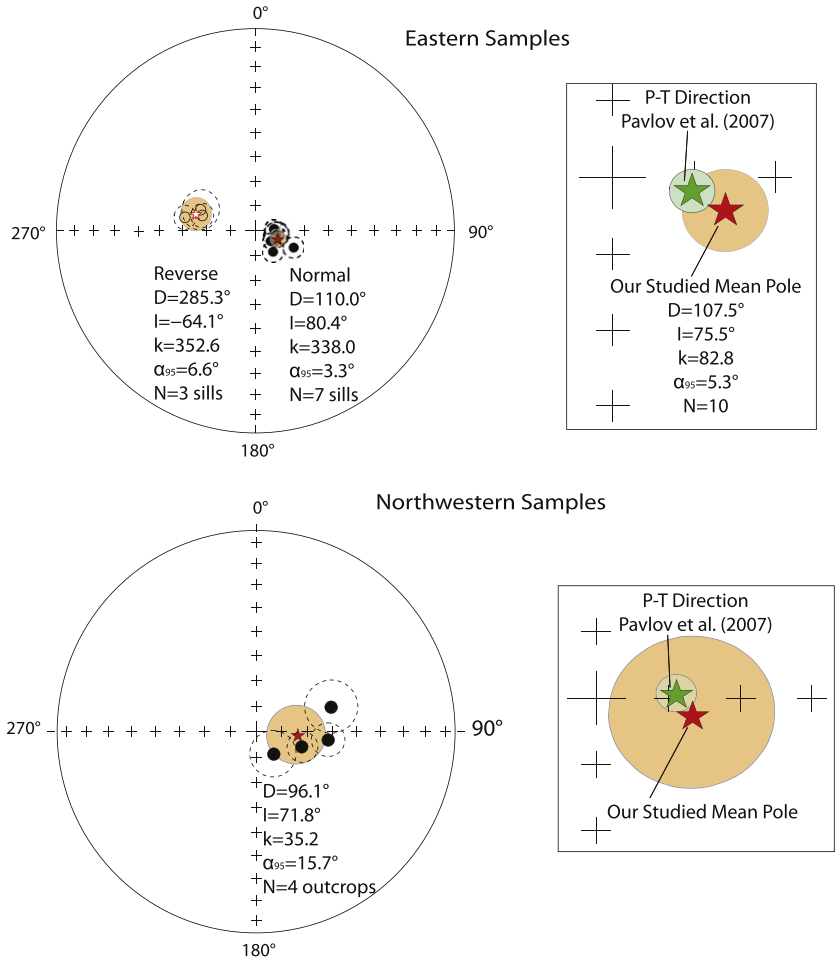

Fig. 5. Equal area projections of primary stable paleomagnetic directions for the eastern and northwestern specimens of the Siberian trap basalts. Closed (open) dots represent positive (negative) inclinations. The red star represents the mean direction for the studied localities. The green star corresponds to the expected mean direction calculated from the Permo–Triassic trap reference paleomagnetic poles from Pavlov et al. (2007). Circles around the directions represent the alpha 95 parameter for each sill/outcrop.

identical. For this reason the quality of the pTRM checks was defined from the mean of the deviations (DEV) between each initial pTRM and the corresponding check over the NRM-TRM segment selected for the calculation of the slope. Nevertheless, in contrast to the calculation of the difference ratio (DRAT) (Selkin and Tauxe, 2000) we did not incorporate any value of the NRM in the calculation of DEV because the NRM is decoupled from the calculation of the pTRM check, which only involves the initial TRM and its repeated measurement. The deviation has been expressed in percentage after normalizing the DEV value, defined as DEV = Σ (pTRM − $\text{pTRM}_{\text{check}}$), with respect to the length of the TRM segment. Similarly, we also calculated the largest deviation (maxDEV) obtained at all steps. The slope of the plots was used to calculate a paleointensity when meanDEV did not exceed 10%.

In accordance with the criteria described above, results have been divided in two categories, "A" and "B". "A" category specimens correspond to results with meanDEV <10%, q > 1, pTRM tail check <20%, a linear segment f > 60% incorporating at least four successive data points, a maximum angular deviation (MAD) of 15°, and β parameter <0.1 (as defined by Selkin and Tauxe, 2000). If one of the previous criteria is not fulfilled the result falls into a "B" category having as limits: 10% < meanDEV < 25%, 20% < pTRM tail check < 25% and 30% < f < 60%. In addition, the multiple-specimen reproducibility criterion, the ratio of the standard deviation of the field estimates to the average of the field for each of the sites, $\sigma_B/\bar{B}$, will be taken into account. This value should be less than 25%, otherwise the average is considered unreliable (Selkin and Tauxe, 2000).

4. Results

4.1. Thermomagnetic and hysteresis measurements

Results from Curie point and thermal dependent MS curves for the three eastern localities are presented in Fig. 2. The heating and cooling thermomagnetic curves are very similar but not exactly identical. The deviations are unlikely to reflect large mineralogical changes, particularly for the second and third specimens (Fig. 2). The first two specimens are characterized by Curie temperatures of ~560 °C, typical of magnetite with very low titanium content. The last specimen has a Curie temperature of 500 °C, implying a larger amount of titanium. Specimens with non-reversible heating and cooling thermomagnetic curves or titanomagnetite with high titanium content have not been selected for the paleointensity experiments. Magnetic hysteresis curves are also shown in Fig. 2. The hysteresis parameters are compatible with those of specimens containing predominantly pseudo-single domain (PSD) particles. The M_{rs}/M_s and H_{cr}/H_c ratios were plotted on a Day diagram in Fig. 3 (Dunlop, 2002). Magnetite single domain (SD) and

Table 1
Late Permian – Early Triassic basalt mean directions of the high temperature primary stable component of NRM for the Eastern Siberian traps (Aikhal (66.17°N, 111.33° E), Sytikanskaya (66.11°N, 111.80°E), Yubileinaya (66.0°N, 111.7°E) kimberlite mine pit areas) and northwestern Noril'sk sill intrusions (69.21°N, 88.03°E). N is the number of directions for specimens or sites accepted for calculation; D (I) is the declination (inclination) of the NRM in geographic (g) or stratigraphic (s) system of coordinates; k, α_{95} – precision parameter and half angle radius of the 95% probability confidence cone.

Sill nomenclature	N	Dg (°)	Ig (°)	Ds. (°)	Is (°)	k	α_{95}(°)	Notes
Aikhal mine pit area								
A1	26	113.3	73.2	–	–	46.0	4.2	Sill near Aikhal kimberlite mine pit
A2	27	102.9	80.2	–	–	78.4	3.2	Aikhal kimberlite mine pit (already published by Kravchinsky et al., 2002)
A3	12	139.1	79.0	–	–	109.2	4.2	Sill near Aikhal kimberlite mine pit
Average	65	118.1	77.8	–	–	236.1	8.0	
Yubileinaya mine pit area								
Y1	22	97.4	81.2	–	–	42.7	4.8	Sill near Yubileinaya kimberlite mine pit
Y2	21	84.0	82.4	–	–	75.8	3.7	Yubileinaya kimberlite mine pit (already published by Kravchinsky et al., 2002)
Y3	15	100.2	81.4	–	–	58.4	5.0	Sill near Yubileinaya kimberlite mine pit
Y4	15	122.4	82.5	–	–	155.5	3.1	Sill near Yubileinaya kimberlite mine pit
Average	73	100.7	82.1	–	–	1298.8	2.6	
Mean for normal polarity sites	7 sills	110.0	80.4	–	–	338.0	3.3	Aikhal and Yubileinaya sites combined
Sytikanskaya mine pit area								
S1	16	280.6	−59.8	–	–	61.5	4.7	Sytikanskaya kimberlite mine pit (already published by Kravchinsky et al., 2002)
S2	8	290.5	−65.4	–	–	50.1	7.9	Sill near Sytikanskaya kimberlite mine pit
S3	20	285.7	−66.8	–	–	46.4	4.8	Sill near Sytikanskaya kimberlite mine pit
Average	44	285.3	−64.1	–	–	352.6	6.6	
Mean for reverse polarity sites	3 sills	285.3	−64.1	–	–	352.6	6.6	Sytikanskaya sites combined
Mean for Aikhal, Yubileinaya and Sytikanskaya sills								
	10 sills	107.5	75.5	–	–	82.8	5.3	
Noril'sk intrusion								
N1	14	160.6	80.7	291.9	84.3	11.5	12.3	
N2	7	92.7	67.9	44.1	88.0	47.4	8.9	
N3	11	73.6	58.6	101.3	73.9	14.2	12.6	
N4	4	110.4	72.0	162.7	75.4	144.8	7.7	
Mean for Noril'sk intrusion	4 Outcrops	96.1	71.8	–	–	35.2	15.7	

superparamagnetic (SP) and single domain and multidomain (MD) theoretical mixing lines of Dunlop (2002) are plotted as a reference. The magnetic grain size corresponds to the PSD region with specimens lying close to the mixing line of SD and MD grain sizes. For paleointensity experiments SD and PSD are the preferable grain sizes.

4.2. Directions

Typical vector end-point diagrams (Zijderveld, 1967) of specimens from 10 sills of the Aikhal, Sytikanskaya, Yubileinaya and four outcrops of the Noril'sk trap differential intrusion are shown in Fig. 4. Secondary viscous components of magnetization were removed after 100 °C for all basalts except Sytikanskaya where heating above 200–300 °C is necessary to remove the secondary component. The mean direction of the high temperature (HT) primary stable component of NRM for all four studied localities is plotted in Fig. 5 and listed in Table 1. The Aikhal, Yubileinaya and Noril'sk localities have a normal polarity and Sytikanskaya has a reverse polarity direction. Mean paleodirections for normal (D = 110.0°, I = 80.4°, k = 338.0, α_{95} = 3.3, N = 7 sills) and reverse (D = 285.3°, I = −64.1°, k = 352.6, α_{95} = 6.6, N = 3 sills) sites were calculated and plotted in Fig. 5. The confidence circles of individual sills overlap each other even when two sets of directions (normal and reverse polarity) exclude the mean of the other. The presence of two antipodal polarities confirms the result reported by Kravchinsky et al. (2002) and is an additional indication for the primary origin of the remanence. The mean directions from the eastern (normal and reverse polarities) (D = 107.5°, I = 75.5°, k = 82.8, α_{95} = 5.3°, N = 10 sills) and northwestern (D = 96.1°, I = 71.8°, k = 35.2, α_{95} = 15.7°, N = 4 outcrops) localities are in excellent agreement with the directions and range of uncertainties derived from the Pavlov et al. (2007) NSP3 paleomagnetic pole (57.0°N, 148.1°E, N = 6, K = 159, A_{95} = 5.3) (estimated values are D = 100.6°, I = 80.1°, α_{95} = 2.8° for eastern localities and D = 84.7°, I = 74.9°, α_{95} = 3.0° for the northwestern locality). The good agreement between the paleomagnetic directions corroborate the ∼250 Ma ages of our specimens.

4.3. Absolute paleointensity

Typical accepted Arai plots are shown in Fig. 6 along with the variations of the NRM intensity as a function of temperature, for specimens that met the criteria described in the methodology section. In accordance with recent studies conducted on historical lava flows (Valet et al., 2010) the suitable specimens are characterized by a sharp decrease of the NRM at high temperatures, which defines the length of the NRM-TRM segment that has been used to calculate the slope. The results of absolute paleointensity have been summarized in Table 2. Twenty-three out of 341 specimens (82 Aikhal, 104 Noril'sk, 73 Sytikanskaya and 82 Yubileinaya) were characterized by acceptable Arai diagrams, but only eight specimens strictly satisfy the criteria in terms of deviations of their pTRM checks with a mean DEV lower than 10%. Northwestern specimens (Noril'sk) did not meet the reliability criteria described above and have been rejected from the final results. All the accepted sites had a parameter $\sigma_B/\bar{B}$ less than 25% (Aikhal: 9.67%, Sytikanskaya: 13.29%, Yubileinaya: 6.00%). The mean geomagnetic field intensity for the three eastern sites obtained from "A" category specimens is 38.43 ± 3.01 μT, a result that agrees within the error with the value of 44.93 ± 4.05 μT derived from the "B" category specimens. We are thus confident that the category B specimens have not been biased by significant changes in magnetic mineralogy during the experiments. The mean paleointensity for

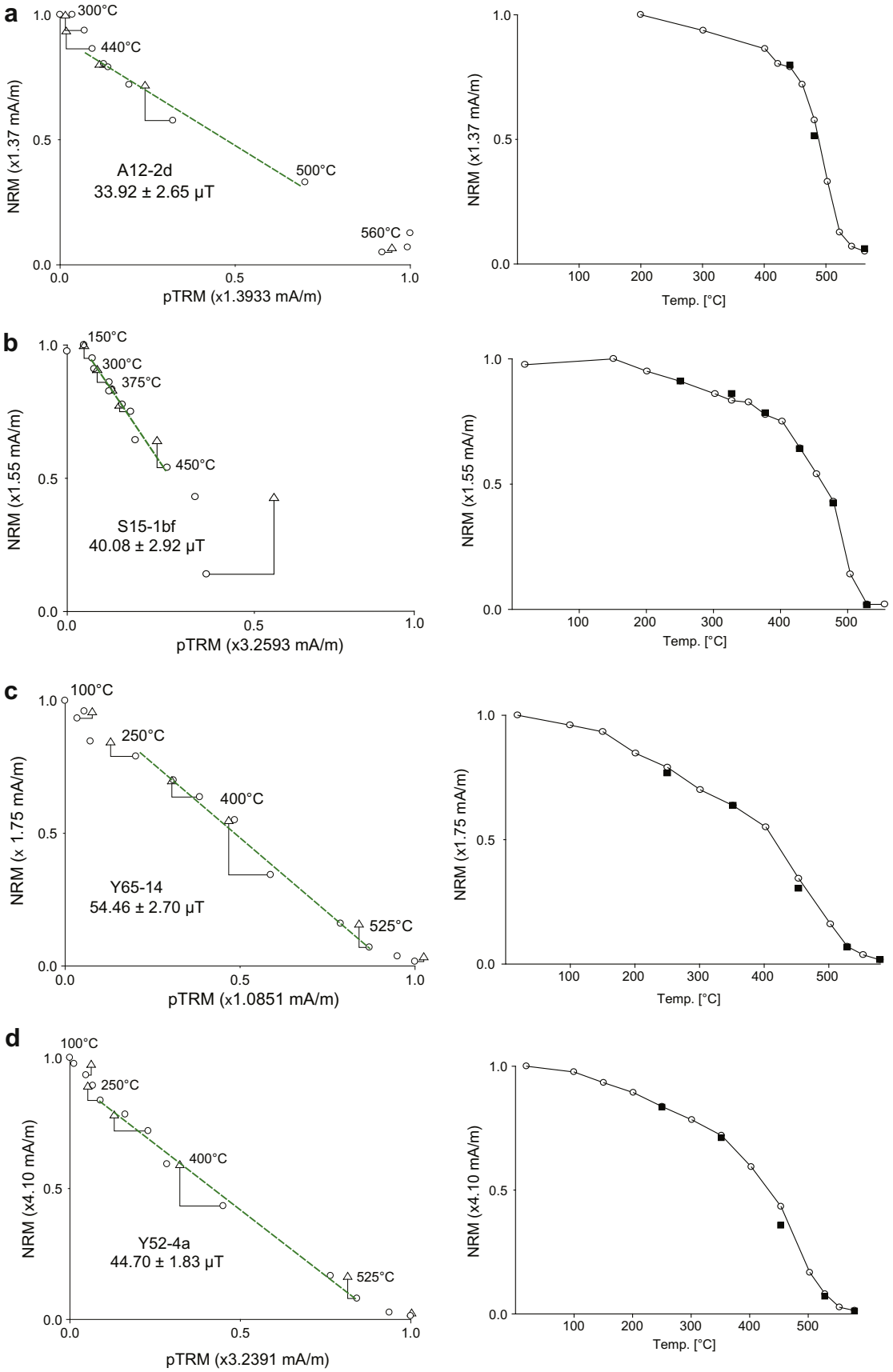

Fig. 6. Typical examples of the paleointensity results for some specimens that met the three criteria listed in the methodology section. NRM vs. pTRM (left hand figures) and NRM as a function of temperature (right hand figures) are shown. Triangles on the NRM vs pTRM plots represent pTRM checks and the faint straight lines represent the temperature interval used for estimating the intensity. Squares on the NRM as a function of temperature plots represent the tail check measurements. (a) Aikhal specimen. (b) Sytikanskaya specimen. (c, d) Yubileinaya specimens. Noril'sk specimens are not presented because they did not fulfill the paleointensity selection criteria.

Table 2
Paleointensity results. Site: Nomenclature for each of the studied sites. Class: Category for each of the samples as defined in the text. ΔT: Temperature range of the linear segment. Protocol: Paleointensity protocol applied: ZI, Coe protocol; IZ, Atkin protocol. $B_{lab:}$ applied laboratory magnetic field. *N*: number of successive data points used for paleointensity calculations. β: Measure of linearity (Selkin and Tauxe, 2000). *f*, *g*, *q* and w are the fraction of the NRM, the gap factor, the quality factor and the weighted factor, respectively, as defined by Coe et al. (1978) and Prévot et al. (1985). MAD: maximum angular deviation. $B \pm \sigma_{b:}$ paleointensity result with its associated standard deviation. VDM $\pm \sigma_{VDM}$: virtual dipolar moment and its associated standard deviation.

Site	Class	ΔT (°C)	Protocol	B_{lab} (μT)	N	β	*f*	*g*	*q*	*w*	MAD(P)	meanDEV(%)	maxDEV(%)	B ± σb(μT)	VDM ± σVDM (x10^22Am²)
Aikhal															
A2-15c	B	250–525	ZI	25	7	0.05	0.84	0.63	10.40	4.70	1.12	23.0	33.5	49.47 ± 2.53	6.81 ± 0.63
A03-8a	B	200–475	IZ	50	7	0.08	0.55	0.75	5.10	2.30	5.15	10.0	12.5	47.09 ± 3.83	6.48 ± 0.72
A04-7a	A	300–520	IZ	50	8	0.05	0.77	0.78	12.60	5.10	7.81	4.4	7.5	34.77 ± 1.65	4.79 ± 0.43
A08-1B	B	400–550	ZI	30	5	0.1	0.57	0.67	2.00	1.20	2.09	14.0	24.0	54.75 ± 10.4	7.54 ± 0.15
A10-3a	B	400–525	ZI	35	4	0.08	0.82	0.371	3.95	2.79	0.85	12.0	18.0	28.93 ± 2.24	3.98 ± 0.43
A12-2a	B	200–475	IZ	50	7	0.1	0.55	0.75	4.00	1.80	5.44	13.0	17.0	61.40 ± 6.41	8.46 ± 0.11
A12-2d	A	400–520	ZI	40	7	0.05	0.82	0.728	11.28	5.05	1.44	9.5	16.0	31.27 ± 1.65	4.31 ± 0.40
A17-7a	B	200–475	IZ	50	7	0.1	0.57	0.62	3.10	1.40	5.65	9.0	12.0	53.21 ± 6.13	7.33 ± 0.10
													Average	45.11 ± 4.36	6.21 ± 0.78
Sytikanskaya															
S8-9a	A	450–575	ZI	30	5	0.1	0.95	0.49	3.80	2.20	2.36	7.0	24.0	17.96 ± 2.21	2.91 ± 0.44
S15-1bf	B	200–450	IZ	40	9	0.07	0.38	0.796	4.20	1.59	2.71	11.0	21.0	40.08 ± 2.92	6.50 ± 0.73
S28-5b2	B	350–575	ZI	25	7	0.07	0.86	0.77	9.10	4.10	1.99	18.0	57.0	27.98 ± 2.04	4.54 ± 0.51
S32-4b	B	375–475	ZI	40	5	0.1	0.32	0.72	1.40	0.80	4.86	19.0	28.0	40.78 ± 6.77	6.61 ± 0.12
S32-4bf	B	375–500	IZ	40	6	0.1	0.49	0.79	2.00	1.00	2.35	9.5	15.2	49.28 ± 9.46	7.99 ± 0.17
													Average	35.22 ± 4.68	5.71 ± 0.92
Yubileinaya															
Y51-3b	A	250–550	ZI	80	7	0.02	0.87	0.76	24.40	10.90	3.36	4.2	10.0	36.25 ± 0.98	4.82 ± 0.16
Y52-3a	A	300–525	IZ	40	10	0.1	0.89	0.77	4.40	1.50	2.82	3.2	6.8	44.90 ± 7.14	5.97 ± 0.95
Y52-4a	B	250–525	ZI	35	7	0.04	0.82	0.76	15.30	6.80	2.42	20.0	35.0	44.70 ± 1.83	5.94 ± 0.26
Y57-6b	B	200–525	ZI	35	8	0.04	0.93	0.79	17.90	7.30	1.78	12.0	28.2	41.03 ± 1.67	5.45 ± 0.24
Y57-6c	B	200–500	ZI	30	7	0.04	0.89	0.79	16.70	7.50	208	16.0	34.0	40.33 ± 1.69	5.36 ± 0.24
Y58-2a	A	150–475	IZ	40	11	0.09	0.84	0.86	8.40	2.80	4.81	7.0	14.4	39.48 ± 3.4	5.25 ± 0.46
Y58-1b	B	150–525	ZI	35	9	0.03	0.86	0.85	27.50	10.40	2.25	13.0	17.0	44.88 ± 1.18	5.97 ± 0.19
Y65-14	B	100–575	ZI	30	12	0.03	0.96	0.88	24.40	7.70	2.25	12.0	42.0	48.98 ± 1.69	6.51 ± 0.25
Y71-3aa	A	100–525	IZ	50	13	0.06	0.86	0.86	12.60	3.80	3.23	8.0	24.0	60.82 ± 3.54	8.08 ± 0.49
Y71-3b	A	200–550	IZ	40	13	0.08	0.78	0.871	8.28	2.50	3.87	5.0	8.0	42.02 ± 3.47	5.59 ± 0.47
													Average	44.34 ± 2.66	5.89 ± 0.37
Total Ave.														42.62 ± 3.69	6.01 ± 1.45

the whole category A and B dataset is 42.62 ± 3.69 μT, which corresponds to a mean virtual dipole moment (VDM) of 6.01 ± 1.45 × 10^{22} Am^2.

5. Discussion

The average paleointensity from our study for eastern localities is approximately 50% larger than previous studies obtained at the northwest of the province (19.3 ± 7.2 μT by Heunemann et al. (2004), and 14.5 ± 1.1 μT by Shcherbakova et al. (2005)). Our results imply that the magnetic field intensity during the Permo-Triassic boundary is similar to the present day variability and that the Mesozoic dipole low could not be straight forwardly extended to the Permo-Triassic boundary.

The suitability of the determinations is constrained by the selection of specimens with high unblocking temperatures. The NRM–TRM diagrams (Fig. 6) do not show any curvature in the analyzed segments which represent at least 60% of the magnetization and more than 80% for the A category specimens, confirming that the specimens are not influenced by MD grains. Furthermore, all specimens that exhibited mineralogical changes during the heating and cooling curves were rejected from the analysis. In addition, 13 of the accepted results follow the ZI protocol and 10 the IZ protocol (Table 2). Our results do not present any significant difference between the two protocols; on the contrary they consistently agree within each other. Moreover, the paleomagnetic directions were stable and corresponded to the expected mean values from Kravchinsky et al. (2002) and Pavlov et al. (2007), confirming that the observed vectors represent the primary magnetization.

The possible presence of MD grains in the northwestern specimens might help to explain the differences in our new and previous paleointensity results for the STB. Shcherbakova et al. (2005) provide evidence for the presence of MD grains indicated by the low temperature segments of the Arai plot of specimens from the Noril'sk area (Table 2, Fig. 4 and the analysis description in their article). Such features might lead to underestimations of the paleointensity values by 10% (Shcherbakova et al., 2005).

Theory and experiments suggest that longer cooling periods for specimens with PSD or MD grains could yield underestimated paleointensity values (Brown, 1984; Winklhofer et al., 1997; Yu, 2011). Differences in cooling rate would only explain the discrepancy between our palaeointensity results for the eastern localities and the previous results for the northwestern localities if the cooling rate of our specimens was faster than that of the northwestern specimens in the previous studies. However, we believe the cooling rate for our specimens was either similar or slower than that of the northwestern specimens in the previous studies. Our specimens come from near surface intrusions (the studied volcanic area preserves the conical structures of the kimberlite pipes which are typical near surface kimberlite structures), whereas the northwestern specimens in the previous studies are extrusive basalts. Thus we believe the higher palaeointensity values in our study are real. Moreover, our paleointensity results from the three studied localities are fairly consistent with each other. Significantly, the paleointensity results for both the normal (Aikhal and Yubileinaya) and reverse (Sytikanskaya) polarity localities are higher than those for previous studies, which adds support to our argument that the geomagnetic dipole low is not characteristic of the STB.

6. Conclusions

In this study we report the first paleointensity results for the eastern part of the Siberian trap basalt province. Paleomagnetic directions from the eastern ($D = 107.5°$, $I = 75.5°$, $k = 82.8$, $\alpha_{95} = 5.3°$, $N = 10$ sills) and northwestern ($D = 95.1°$, $I = 71.8°$, $k = 35.2$, $\alpha_{95} = 15.7°$, $N = 4$ outcrops) localities are in excellent agreement with the expected directions calculated from the reference paleomagnetic poles of Pavlov et al. (2007) ($D = 100.6°$, $I = 80.1°$, $\alpha_{95} = 2.8°$ for the eastern localities and $D = 84.7°$, $I = 74.9°$, $\alpha_{95} = 3.0°$ for the northwestern locality), confirming that the age interval of our specimens correspond to the Permo-Triassic boundary. The northwestern specimens did not meet our reliability criteria for paleointensity and were not used for further analysis. The eastern locality results have distinctly higher VDM values ($6.01 \pm 1.45 \times 10^{22}$ Am^2) compared to previous studies (Heunemann et al., 2004; Shcherbakova et al., 2005) suggesting: (1) a low intensity of the magnetic field is not characteristic during the Permo-Triassic boundary; and (2) the Mesozoic dipole low cannot be extended until this period of time. Discrepancies between the present results and previous studies could possibly be explained by the existence of multidomain grains in the northwestern specimens of the previous studies. Our mineralogical experiments did not reveal the presence of multidomain grains in the selected specimens for paleointensity analysis. Our results suggest that the geomagnetic field intensity at the Permo-Triassic boundary was very close to the observed present-day values.

Acknowledgments

We thank L.P. Koukar, L. Tober and L. Duerksen for their help during laboratory measurements and J.I. Savrasov, A.N. Zhitkov and A.Ya. Kravchinsky for their help during field work in 1975, 1979, 1984–85 and 1995–96. The study was partially funded by support for V.A.K. from the Natural Sciences and Engineering Research Council of Canada (NSERC). We thank Lisa Tauxe and the other two anonymous reviewers for their helpful comments and suggestions for the improvement of this manuscript. Some of the measurements were performed using V.A.K.'s equipment acquired from the Canadian Foundation for Innovation and the University of Alberta. The VFTB measurements (thermomagnetic curves and hysteresis plots) were performed using D.K.P.'s funds from NSERC.

References

Aitken, M.J., Allsop, A.L., Bussel, G.D., Winter, M.B., 1988. Determination of the intensity of the Earth's magnetic field during archeological times: reliability of the Thellier technique. Rev. Geophys. 26, 3–12.

Almukhamedov, A.I., Medvedev, A.Ya., Mitchell, C., Zolotukhin, V.V., 1996. Flood basalts in the core of the Tunguska syneclinse: comparative geochemistry. Russian Geol. Geophys. Novosibirsk 37, 3–16 (in Russian).

Almukhamedov, A.I., Medvedev, A.Ya., Zolotukhin, V.V., 2004. Compositional evolution of the Permian–Triassic basalts of the Siberian Platform in time and space. Petrology 2 (4), 339–353 (in Russian).

Basu, A.R., Hannigan, R.E., Jacobsen, S.B., 1998. Melting of the Siberian mantle plume. Geophys. Res. Lett. 25, 2209–2212.

Biggin, A.J., Thomas, D.N., 2003. Analysis of long-term variations in the geomagnetic poloidal field intensity and evaluation of their relationship with global geodynamics. Geophys. J. Int. 152, 392–415.

Bol'shakov, A.S., Solodovnikov, G.M., 1983. Geomagnetic field intensity in the Late Jurassic and Early Cretaceous. Izv. Acad. Sci. Phyis. 19, 976–982.

Bol'shakov, A.S., Solodovnikov, G.M., Vinogradov, Y.K., 1989. Paleointensity of the geomagnetic field in the early Permian. Izv., Earth Phys. (Eng. Trans.) 25, 70–78.

Brandt, D., Hartmann, G.A., Yokoyama, E., Catelani, E.L., Trindade, R.I.F., 2009. Paleointensity data from Early Cretaceous Ponta Grossa dikes (Brazil) using a multispecimen method. Earth Planets Space. 61, 41–49.

Brown, E.M., 1984. Experiments on TRM intensity dependence on cooling rate. Geoph. Res. Lett. 3, 205–208.

Coe, R.S., 1967. Paleointensities of the Earth's magnetic field determined from tertiary and quaternary rocks. J. Geophys. Res. 72, 3247–3262.

Coe, R.S., Grommé, S., Mankinen, E.A., 1978. Geomagnetic paleointensities from radiocarbon-dated lava flows an Hawaii and the question of the Pacific nondipole low. J. Geophys. Res. 83, 1740–1756.

Cogné, J.-P., 2003. PaleoMac: a Macintosh™ application for treating paleomagnetic data and making plate reconstructions. Geochem. Geophys. Geosyst. 4 (1), 1007. http://dx.doi.org/10.1029/2001GC000227.

Courtillot, V., Jaupart, C., Manighetti, I., Tapponnier, P., Besse, J., 1999. On causal links between flood basalts and continental breakup. Earth Planet. Sci. Lett. 166, 177–195.

Courtillot, V., Renne, P.R., 2003. On the ages of flood basalt events. C.R. Geosci. 335, 113–140.

Dalrymple, G.B., Czamanske, G.K., Fedorenki, V.A., Simonov, O.N., Lanphere, M.A., Likhachev, A.P., 1995. A reconnaissance $^{40}Ar/^{39}Ar$ geochronologic study of ore-bearing and related rocks, Siberian Russia. Geochim. Cosmochim. Acta 59, 2071–2083.

Dunlop, D.J., 2002. Theory and application of the Day plot (Mrs/Ms vs Hcr/Hc) 1. Theoretical curves and test using titanomagnetite data. J. Geophys. Res. 107, 4–22.

Enkin, R.J., 1996. A computer program package for analysis and presentation of paleomagnetic data, Pacific Geoscience Center, Geological Survey of Canada.

Elkins Tanton, L.T., Hager, B.H., 2000. Melt intrusion as a trigger for lithospheric foundering and the eruption of the Siberian flood basalts. Geophys. Res. Lett. 27, 3937–3940.

Fisher, R., 1953. Dispersion on a sphere. Proceedings Royal Society London. Ser. A 217, 295–305.

Garcia, A., Thomas, N., Liss, D., Shaw, J., 2006. Low geomagnetic field intensity during the Kiaman superchron: Thellier and microwave results from the Great Whin Sill intrusive complex, northern United Kingdom. Geophys. Res. Lett. 33. http://dx.doi.org/10.1029/2006GL026729.

Goguitchaichvili, A., Alva-Valdivia, L.M., Urrutia, J., Morales, J., 2002. On the reliability of Mesozoic Dipole Low: New absolute paleointensity results from Parana flood basalts (Brazil). Geophys. Res. Lett. 29. http://dx.doi.org/10.1029/2002GL015242.

Goguitchaichvili, A., Cejudo Ruiz, R., Sanchez Bettucci, L., Aguilar Reyes, B., Alva-Valdivia, L.M., Urrutia-Fucugauchi, J., Morales, J., Calvo Rathert, M., 2008. New absolute paleointensity results from the Parana Magmatic Province (Uruguay) and the Early Cretaceous geomagnetic paleofield. Geochem., Geophys., Geosyst, 9, doi: 10.1029/2008GC002102.

Griffin, W.L., Ryan, C.G., Kaminsky, F.V., O'Reilly, S.Y., Natapov, L.M., Win, T.T., Kinny, P.D., Ilupin, I.P., 1999. The Siberian lithosphere traverse, mantle terranes and the assembly of the Siberian Craton. Tectonophysics 310, 1–35.

Harcombe-Smee, B.J., Piper, J.D.A., Rolph, T.C., Thomas, D.N., 1996. A palaeomagnetic and palaeointensity study of the Mauchline lavas, south-west Scotland. Phys. Earth Planet. Int. 94, 63–73.

Heller, R., Merrill, R.T., McFadden, P.L., 2002. The variation of intensity of earth's magnetic field with time. Phys. Earth Planet. Int. 131, 237–249.

Herrero–Bervera, E., Valet, J.-P., 2009. Testing determinations of absolute paleointensity from the 1955 and 1960 Hawaiian flows. Earth Planet. Sci. Lett. 287, 420–433.

Heunemann, C., Krasa, D., Soffel, H.C., Gurevitch, E., Bachtadse, V., 2004. Directions and intensities of the Earth's magnetic field during a reversal: results from the Permo–Triassic Siberian trap basalts, Russia. Earth Planet. Sci. Lett. 218, 197–213.

Kirschvink, J.L., 1980. The least-squares line and plane and the analysis of paleomagnetic data. Geophys. J. R. Astron. Soc. 62, 699–718.

Kosterov, A., Perrin, M., Glen, J.M., Coe, R.S., 1998. Paleointensity of the Earth's magnetic field in early Cretaceous time: The Paraná Basalt. Brazil. J. Geophys. Res. 103, 9739–9753.

Kravchinsky, V.A., Konstantinov, K.M., Courtillot, V., Savrasov, J.I., Valet, J.P., Cherniy, S.D., Mishenin, S.G., Parasotka, S., 2002. Palaeomagnetism of the east Siberian traps and kimberlites: two new poles and palaeogeographic reconstruction at about 360 and 250 Ma. Geophys. J. Int. 148, 1–33.

Kuzmin, M.I., Yarmolyuk, V.V., Kravchinsky, V.A., 2010. Phanerozoic hot spot traces and paleogeographic reconstruction of the Siberian continent based on interaction with the African large low shear velocity province. Earth Sci. Rev. 102, 29–59.

McClelland, E., Briden, J.C., 1996. An improved methodology for Thellier-type paleointensity determination in igneous rocks and its usefulness for verifying primary thermoremanence. J. Geophys. Res. 101, 21995–22013.

Pan, Y., Hill, M., Zhu, R., Shaw, J., 2004. Further evidence for low intensity of the geomagnetic field during the early Cretaceous time: using the modified Shaw method and microwave technique. Geophys. J. Int. 157, 553–564.

Pavlov, V.E., Courtillot, V., Bazhenov, M.L., Veselovsky, R.V., 2007. Paleomagnetism of the Siberian traps: new data and new overall 250 Ma pole of Siberia. Tectonophysics 443, 72–92.

Prévot, M., Mankinen, E.A., Coe, R.S., Grommé, C.S., 1985. The Steens mountain (Oregon) geomagnetic polarity transition. 2. Field intensity variations and discussion of reversal models. J. Geophys. Res 90, 10417–10448.

Prévot, M., El–Messaoud Derder, M., McWilliams, M., Thompson, J., 1990. Intensity of the Earth's magnetic field: evidence for a mesozoic dipole low. Earth Planet. Sci. Lett. 97, 129–139.

Perrin, M., Prevot, M., Mankinen, E.A., 1991. Low intensity of the geomagnetic field in early Jurassic time. J. Geophys. Res. 96, 14197–14210.

Perrin, M., Shcherbakov, V., 1997. Paleointensity of the Earth's magnetic field for the past 400 Ma: evidence for a dipole structure during the mesozoic low. Journal of Geomagnetism and Geoelectricity 49, 601–614.

Reichow, M.K., Saunders, A.D., White, R.V., Almukhamedov, A.I., Medvedev, A.Ya., 2005. Geochemistry and petrogenesis of basalts from the West Siberian Basin: an extension of Permo-Triassic Siberian Traps, Russia. Lithos 79, 425–452.

Reichow, M.K., Pringle, M.S., Al'Mukhamedov, A.I., Allen, M.B., Andreichev, V.L., Buslov, M.M., Davies, C.E., Fedoseer, G.S., Fitton, J.G., Inger, S., Medvedev, A.Ya., Mitchell, C., Puchkov, V.N., Safonava, I.Yu., Scoot, R.A., Saunders, A.D., 2009. The timing and the extent of the eruption of the Siberian traps large igneous province. Implications for the end-Permian environmental crisis. Earth and Planetary Science Letters 227, 9–20.

Riisager, P., Riisager, J., 2001. Detecting multidomain magnetic grains in Thellier palaeointensity experiments. Phys. Earth Planet. Int. 125, 111–117.

Ruiz, R.C., Goguitchaichvili, A., Geuna, S.E., Alva-Valdivia, L.M., Sole, J., Morales, J., 2006. Early cretaceous absolute geomagnetic paleointensities from Córdoba Province (Argentina). Earth Planets Space 58, 1333–1339.

Saunders, A.D., Englend, R.W., Reichow, M.K., White, R.W., 2005. A mantle plume origin for the Siberian traps: uplift and extension in the West Siberian Basin, Russia. Lithos 79, 407–424.

Senanayake, W.E., McElhinny, M.W., 1983. A paleointensity method for use with highly oxidized basalts, and application to some Permian volcanics. Journal of Geophysics 52, 85–96.

Selkin, P.A., Tauxe, L., 2000. Long-term variations in paleointensity. Phil. Trans. R. Soc. Lond. 358, 1065–1088.

Selkin, P.A., Gee, J.S., Tauxe, L., 2007. Nonlinear thermoremanence acquisition and implications for paleointensity data. Earth and Planetary Science Letters 256, 81–89.

Shaar, R., Ron, H., Tauxe, L., Kessel, R., Agnon, A., Ben-Yosef, E., Feinberg, J.M., 2010. Testing the accuracy of absolute intensity estimates of the ancient geomagnetic field using copper slag material. Earth and Planetary Science Letters 290, 201–213.

Shcherbakova, V.V., Shcherbakov, V.P., Vodovozov, V.V., Sycheva, N.K., 2005. Paleointensity at the Permian–Triassic boundary and in the late Permian. Izv. Acad. Sci. Phys. Solid Earth 41, 931–944.

Shcherbakova, V.V., Perrin, M., Shcherbakov, V.P., Pavlov, V.E., Ayvaz'yan, A., Zhidkov, G.V., 2009. Rock Magnetic and paleointensity results from mesozoic baked contacts of Armenia. Earth Planets Space 61, 23–39.

Solodovnikov, G.M., 1992. Paleointensity of the gomagnetic field in the lower Permian. Izv., Earth Phys. (Eng. Trans.) 28, 718–722.

Solodovnikov, G.M., 1995. Paleointensity of the early Triassic geomagnetic field. Izv., Earth Phys. (Eng. Trans.) 30, 815–821.

Tanaka, H., Kono, M., Uchimura, H., 1995. Some global features of paleointensity in geological time. Geophysical Journal International 120, 97–102.

Tarduno, J.A., Cottrell, R.D., 2005. Dipole strength and variation of the time-averaged reversing and nonreversing geodynamo based on Thellier analyses of single plagioclase crystals. Journal of Geophysical Research 110. http://dx.doi.org/10.1029/2005JB003970.

Tauxe, L., 2006. Long-term trends in paleointensity: The contribution of DSDP/ODP submarine basaltic glass collections. Phys. Earth Planet. Int. 156, 223–241.

Thellier, E., Thellier, O., 1959. Sur l'intensité du champ magnétique terrestre dans le passé historique et géologique. Annales Geophysicae 15, 285–376.

Thomas, D.N., Rolph, T.C., Shaw, J., 1995. Palaeointensity results from the Permo-Carboniferous (Kiaman) reversed superchron: the Great Whin and Midland Valley sills of the northern United Kingdom. Geophysical Journal International 123, 798–816.

Thomas, D.N., Rolph, T.C., Friel, D.F., 1997. Permo-Carboniferous (Kiaman) paleointensity results from the western Bohemian Massif Germany. Geophysical Journal International 130, 257–265.

Valet, J.P., Tric, E., Herrero–Bervera, E., Meynadier, L., Lockwood, J.P., 1998. Absolute paleointensity from Hawaiian lavas younger than 35 ka. Earth Planet. Sci. Lett. 161, 19–32.

Valet, J.-P., Herrero-Bervera, E., Carlut, J., Kondopoulou, D., 2010. A selective procedure for absolute paleointensity in lava flows. Geophysical Research Letters 37. http://dx.doi.org/10.1029/2010GL044100.

Vandamme, D., Courtillot, V., 1992. Paleomagnetic constraints on the structure of the Deccan traps. Phys. Earth and Planet. Int 74, 241–261.

Winklhofer, M., Fabian, K., Heider, F., 1997. Magnetic blocking temperatures of magnetite calculated with a three-dimensional micromagnetic model. J. Geophys. Res., 102, 22,695–22,709.

Yu, Y., Tauxe, L., Gee, J.S., 2007. A linear field dependence of thermoremanence in low magnetic fields. Phys. Earth Planet. Int. 162, 244–248.

Yu, Y., 2011. Importance of cooling rate dependence of thermoremanence in paleointensity determination. Journal of Geophysical Research 116, B09101. http://dx.doi.org/10.1029/2011JB008388.

Zhu, R., Pan, Y., Shaw, J., Li, D., Li, Q., 2001. Geomagnetic palaeointensity just prior to the Cretaceous normal superchron. Phys. Earth Planet. Int. 128, 207–222.

Zhu, R., Hoffman, K.A., Pan, Y., Shi, R., Li, D., 2003. Evidence for weak geomagnetic field intensity prior to the Cretaceous normal superchron. Phys. Earth Planet. Int. 136, 187–199.

Zijderveld, J.D.A., 1967. A.C. demagnetization of rocks, analysis of results. In: Methods in paleomagnetism, D.W. Collinson, K.M. Creer, and S.K. Runcorn, eds., Elsevier, Amsterdam, 254–286.